JOURNAL OF VIROLOGY, Nov. 2005, p. 13399–13411 Vol. 79, No. 21
0022-538X/05/$08.00+0 doi:10.1128/JVI.79.21.13399–13411.2005

The nsp2 Replicase Proteins of Murine Hepatitis Virus and Severe Acute Respiratory Syndrome Coronavirus Are Dispensable for Viral Replication

Rachel L. Graham,[2,3] Amy C. Sims,[4] Sarah M. Brockway,[2,3] Ralph S. Baric,[4] and Mark R. Denison[1,2,3]*

Departments of Pediatrics[1] and Microbiology and Immunology[2] and Elizabeth B. Lamb Center for Pediatric Research,[3] Vanderbilt University Medical Center, Nashville, Tennessee, and Department of Epidemiology, School of Public Health, University of North Carolina, Chapel Hill, North Carolina[4]

Received 21 June 2005/Accepted 9 August 2005

The positive-stranded RNA genome of the coronaviruses is translated from ORF1 to yield polyproteins that are proteolytically processed into intermediate and mature nonstructural proteins (nsps). Murine hepatitis virus (MHV) and severe acute respiratory syndrome coronavirus (SARS-CoV) polyproteins incorporate 16 protein domains (nsps), with nsp1 and nsp2 being the most variable among the coronaviruses and having no experimentally confirmed or predicted functions in replication. To determine if nsp2 is essential for viral replication, MHV and SARS-CoV genome RNA was generated with deletions of the nsp2 coding sequence (MHVΔnsp2 and SARSΔnsp2, respectively). Infectious MHVΔnsp2 and SARSΔnsp2 viruses recovered from electroporated cells had 0.5 to 1 $\log_{10}$ reductions in peak titers in single-cycle growth assays, as well as a reduction in viral RNA synthesis that was not specific for any positive-stranded RNA species. The Δnsp2 mutant viruses lacked expression of both nsp2 and an nsp2-nsp3 precursor, but cleaved the engineered chimeric nsp1-nsp3 cleavage site as efficiently as the native nsp1-nsp2 cleavage site. Replication complexes in MHVΔnsp2-infected cells lacked nsp2 but were morphologically indistinguishable from those of wild-type MHV by immunofluorescence. nsp2 expressed in cells by stable retroviral transduction was specifically recruited to viral replication complexes upon infection with MHVΔnsp2. These results demonstrate that while nsp2 of MHV and SARS-CoV is dispensable for viral replication in cell culture, deletion of the nsp2 coding sequence attenuates viral growth and RNA synthesis. These findings also provide a system for the study of determinants of nsp targeting and function.

Positive-stranded RNA viruses express polyproteins from their input genome RNA that are proteolytically processed by viral and cellular proteinases to yield nonstructural proteins, structural proteins, or both. This strategy results in evolutionary, organizational, and functional linkages between protein domains at the levels of RNA sequence, protein translation, proteolytic processing at specific cleavage sites, and functions of intermediate precursor proteins and mature proteins. The multiple points of regulation present a formidable theoretical barrier to extensive deletions or insertions in polyproteins. Several groups working with positive-stranded RNA viruses have reported deletions of portions of protein domains or the generation of viruses whose extensive defects in replication require rescue by replicons or helper viruses (16, 26, 29, 32, 34, 38, 39, 44, 48). However, for animal positive-stranded RNA viruses, we have identified no published reports of autonomously replicating mutant viruses with deletions of complete mature protein domains within polyproteins. Thus, the available experimental evidence has suggested that structural and functional features of positive-stranded RNA virus polyprotein domains are essential for virus replication.

* Corresponding author. Mailing address: Department of Pediatrics, Vanderbilt University Medical Center, D6217 MCN, Nashville, TN 37232-2581. Phone: (615) 343-9881. Fax: (615) 343-9723. E-mail: mark.denison@vanderbilt.edu.

Coronaviruses contain 27- to 32-kb positive-stranded RNA genomes (Fig. 1). The 5′-most open reading frame (ORF), ORF1, also referred to as the replicase gene, is translated in the host cell cytoplasm into ORF1a and ORF1ab polyproteins containing up to 16 protein domains that are co- and post-translationally processed by virus-encoded proteinases into intermediate precursors and mature nonstructural proteins (nsps). All analyzed nsps of murine hepatitis virus (MHV) and severe acute respiratory syndrome coronavirus (SARS-CoV) localize to virus-induced cytoplasmic double-membrane vesicles that are the sites of viral RNA synthesis and are referred to as replication complexes (18, 36).

Based on the numbering of nsps reported for SARS-CoV, the orthologs of coronavirus nsps serve confirmed (nsps 3, 5, 12, and 13), predicted (nsps 12, 14, 15, and 16), or unknown (nsps 1, 2, 4, 6, and 7 to 10) functions in replication as well as possible roles in virus-host interactions (nsps 1, 3, 4, and 6) and virulence (nsp14). In ORF1a, nsp3 encodes either one or two papain-like proteinases (PLPs), and nsp5 is a 3C-like proteinase (1, 30). ORF1b encodes of the putative viral RNA-dependent RNA polymerase (nsp12), helicase (nsp13), and RNA-processing enzymes: a putative 3′-5′ exonuclease (nsp14), a poly(U)-specific endonuclease (nsp15), and a putative ribose 2′-*O*-methyltransferase (nsp16) (17, 23, 24, 28, 42). In addition, an MHV nsp14 mutant retains wild-type growth in culture but is attenuated for replication and virulence in mice, suggesting that nsp14 has specific roles in pathogenesis (43).

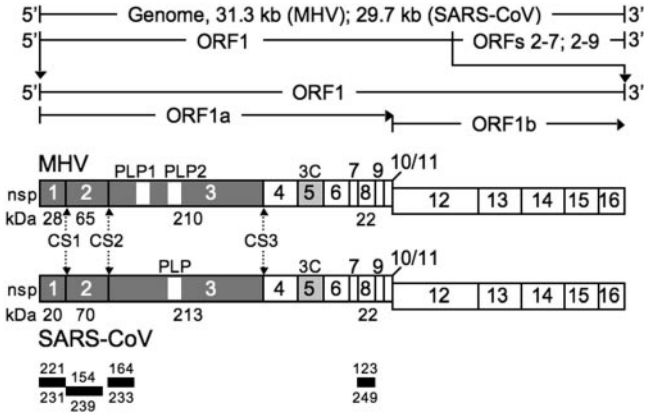

FIG. 1. MHV and SARS-CoV ORF1 organization. The MHV genome is 31.3 kb in length, and the SARS-CoV genome is 29.7 kb in length. ORF1 comprises 21.7 kb of the MHV genome and 21.5 kb of the SARS-CoV genome. MHV contains six downstream ORFs (ORFs 2 to 7), and SARS-CoV contains eight downstream ORFs (ORFs 2 to 9). Schematics are not to scale. ORF1 is translated into a ~500-kDa ORF1a polyprotein (major product) or an ~800-kDa ORF1ab polyprotein (minor product). The mature protein domains of ORF1ab are indicated with nonstructural protein (nsp) numbers. Papain-like proteinase domains (PLP1 and PLP2 for MHV, PLP for SARS-CoV; white boxes within nsp3) process nsps 1, 2, and 3 (indicated in dark gray), and 3C-like proteinases (3C, light gray box, nsp5) process nsps 4 to 16. The molecular masses of nsps 1, 2, 3, and 8 are indicated, in kDa, below the proteins, and papain-like proteinase cleavage sites 1 to 3 (CS1, CS2, and CS3) are indicated. Black bars beneath the schematic indicate proteins generated to induce the rabbit polyclonal antibodies used in this study. Antibody numbers (VU prefix) are given for MHV above the bars and for SARS-CoV below the bars.

Coronaviruses are divided into three groups (groups 1, 2, and 3) based on comparisons of serotype specificity and genome organization, with MHV as a prototype group 2 coronavirus. Amino acid sequence identity of replicase polyproteins from different groups varies from less than 30% to over 60% (37), with the most variability occurring in the protein domains upstream of the nsp3 orthologs. Variability in this region includes differences in the sizes of nsps 1 and 2 as well as in amino acid sequence identity, with the most variation observed between coronavirus groups rather than among different coronaviruses within a given group. Because nsps 1, 2, and 3 are processed by one or two papain-like proteinases in nsp3, it has been suggested that the proteins encoded in this region have coevolved with nsp3 and may mediate group- and/or host-specific functions within the viral life cycle (12, 53, 54).

SARS-CoV is most closely related to group 2 coronaviruses such as MHV in identity and similarity from nsp4 through nsp16 (Fig. 1) (19, 37, 42). In addition, SARS-CoV retains the general organization and sizes of nsps 1, 2, and 3 most similar to group 2 coronaviruses (42, 46). However, there also are important differences between nsps 1, 2, and 3 of MHV and SARS-CoV. First, there is very limited identity or similarity between nsp1 and nsp2 of MHV and SARS-CoV (37). In addition, MHV has two papain-like proteinase activities in nsp3, the first of which (PLP1) mediates cleavage at cleavage site 1 (CS1) between nsp1 and nsp2 and at cleavage site 2 (CS2) between nsp2 and nsp3, and the second of which (PLP2) mediates cleavage at cleavage site 3 (CS3) between nsp3 and nsp4 (3, 15, 22, 25). In contrast, SARS-CoV has only the functional ortholog of PLP2 in nsp3 to mediate all three cleavage events (Fig. 1) (46).

Processing of the nsp 1 to 3 region of group 2 and group 2-like coronaviruses is likely an ordered process consisting of co- and posttranslational processing events. nsp1, a 28-kDa protein previously referred to as p28, is the first protein to be processed from the nascent polyprotein following translation of the proteinase domains within nsp3 (12). nsp2 and nsp3 likely exist as precursor proteins prior to their processing into mature nsp2 and nsp3 products. Due to the large size of this nsp2-3 precursor, previous studies have identified it as a 290-kDa (12) or a 250-kDa (40) product based on migration on sodium dodecyl sulfate (SDS)-polyacrylamide gel electrophoresis (PAGE). Subsequent processing then yields mature nsp2, a 65-kDa product (12, 40), and nsp3, a high-molecular-weight product with a predicted molecular mass of 222 kDa and estimated observed molecular masses of 240 kDa (12) and 210 kDa (40). Similarly sized species have been observed for SARS-CoV, and pulse-chase studies suggest the processing events follow a similar, if not identical, sequential order (19).

Reverse genetic systems for both MHV and SARS-CoV (47, 51, 52) provide a powerful tool to study requirements for protein expression, processing, and function during replication of these two viruses as well as allow direct comparisons of conserved protein domains, processing events, or amino acid residues. The nsp2 protein is an attractive target for genetic studies, since it has been reported that engineered mutations that eliminate cleavage at CS1 between nsp1 and nsp2 yield infectious virus (13), suggesting that nsp2 either retains function in an uncleaved form or has a function that is dispensable for viral replication. Still, it is not known if nsp2, either as a mature protein or as a component of the coronavirus polyprotein, is absolutely required for viral replication.

In the present study, we sought to determine whether the nsp2 proteins of the coronaviruses MHV-A59 (hereafter MHV) and SARS-CoV were required for viral replication or for processing at the flanking cleavage sites. Reverse genetic deletion of the nsp2 domains of the MHV and SARS-CoV polyproteins allowed recovery of infectious mutants with defects in growth and RNA synthesis and demonstrated intact polyprotein processing, including cleavage at engineered chimeric nsp1/3 cleavage sites. Taken together, these results demonstrate that the nsp2 domains of the MHV and SARS-CoV replicase polyproteins are not required for viral replication. These results suggest that there is significant structural and functional flexibility within the coronavirus polyprotein and that ORF1 encodes at least one and perhaps several protein domains that may be dedicated to functions distinct from production of infectious virus.

MATERIALS AND METHODS

Wild-type virus and cells. Murine hepatitis virus strain A-59 (MHV) or recombinant wild-type murine hepatitis virus (MHV-wtic) (13, 43) was used as the wild-type control in all MHV experiments. MHV-A59 reference sequences AY910861 and AY700211 were used for cloning studies. Delayed brain tumor (DBT) cells (21) and baby hamster kidney cells expressing the MHV receptor (BHK-MHVR) (9, 10) were grown in Dulbecco's modified Eagle's medium (DMEM) that contained 10% fetal bovine serum (FBS) for all experiments. Medium for BHK-MHVR cells was supplemented with G418 (0.8 mg/ml) for selection of cells expressing the receptor.

TABLE 1. MHV and SARS-CoV replicase antibodies

Virus	Protein	Antiserum	Protein detected and size (kDa)	Use[a]	Amino acids	Reference
MHV	nsp1	VU221	nsp1 (28)	IP	1–247	7
	nsp2	VU154	nsp2 (65) nsp2-3 (275)	IP, IF	248–521	41
	nsp3	VU164	nsp3 (210) nsp2-3 (275)	IP	833–1179	This report
	nsp8	VU123	nsp8 (22)	IP	4015–4208	5
SARS-CoV	nsp1	VU231	nsp1 (20)	IB	1–227	37
	nsp2	VU239	nsp2 (70)	IB	228–818	37
	nsp3	VU233	nsp3 (213)	IB	819–1154	37
	nsp8	VU249	nsp8 (22)	IB	3920–4117	37

[a] IP, immunoprecipitation; IF, immunofluorescence; IB, immunoblot. Use refers to the application of the antibody in this report.

Severe acute respiratory syndrome coronavirus Urbani strain (SARS-Urbani, or SARS-CoV in this report) and/or assembled wild-type SARS-CoV (SARS-wtic) were used as wild-type controls in all SARS-CoV experiments. SARS-CoV Urbani reference sequence AY278741 was used for cloning studies. African green monkey kidney (Vero-E6) cells were grown in DMEM that contained 10% FBS, kanamycin (0.25 μg/ml), and gentamicin (0.05 μg/ml) for all experiments.

Generation of nsp2-expressing cells. To generate DBT cells stably transduced to express nsp2, the pBabe-puro vector system derived from murine Moloney leukemia virus (33) was used (kindly provided by Chris Aiken, Vanderbilt University). To clone the nsp2 coding sequence (MHV-A59 nucleotides 951 to 2705) into the pBabe-puro vector, PCR was performed using the MHV infectious cDNA fragment A plasmid (pCR-XL-TopoA) (52) as the template. Primers were designed to incorporate translation initiation and translation termination codons flanking the nsp2 sequence as well as restriction sites (5′ SnaBI and 3′ SalI) to facilitate subcloning nsp2 into pBabe-puro.

The sequences of the primers are (sense) 5′-TAC GTA ATG GTT AAG CCC ATC CTG TTT G-3′ and (antisense) 5′-GTC GAC TCA CGC ACA GGG AAA CCT CC-3′. The PCR product was gel purified and cloned into pGEM-T-easy (Promega), and the T7 and SP6 primers were used to sequence across the nsp2 coding region to verify the intended sequence. Primer-generated restriction sites (5′ SnaBI and 3′ SalI) were then used to subclone the nsp2 sequence into the pBabe-puro vector to generate pBabe-nsp2.

To produce replication-defective retroviruses, human 293T cells (approximately 2×10^6 cells) in a 100-mm culture dish were cotransfected with pHCMV-VSVg (encoding the vesicular stomatitis virus envelope glycoprotein), pCL-ampho (encoding Moloney murine leukemia virus *gag* and *pol*), and either pBabe-nsp2 or the pBabe-puro vector using calcium phosphate as previously described (8, 50). The transfected cells were incubated at 35°C for 16 h in DMEM supplemented with 10% FBS to allow calcium phosphate precipitation. The transfection medium was then aspirated and the cells were incubated at 35°C for 48 h in 4 ml of fresh DMEM supplemented with 10% FBS. To harvest retroviral particles, the medium was clarified by centrifugation at 1,000 × *g*, passed through 0.45-μm-pore-size syringe filters, and frozen in aliquots at −80°C. The replication-defective retroviral particles are referred to as VpBabe-nsp2 and VpBabe-vec.

To create nsp2-expressing and vector control cells, DBT cells were grown to 20% confluence in 60-mm cell culture dishes and then transduced with either VpBabe-nsp2 or VpBabe-vec. Equal amounts (1:1) of the filtered retrovirus-containing supernatants and DMEM supplemented with 10% FBS and Polybrene (8 μg/ml) were added to cells in a final volume of 2 ml. The cells were cultured at 37°C for 16 h and then the transduction medium was replaced with fresh warm DMEM supplemented with 10% FBS. At 48 h posttransduction, the cells were transferred to 75-cm flasks and incubated in DMEM supplemented with 10% FBS and puromycin (1 μg/ml) to select cells that had stably integrated the retroviral vectors. Pools of stably transduced cells were maintained in puromycin selection medium for at least 2 weeks prior to assaying expression using immunofluorescence and immunoprecipitation assays (not shown). DBT cells stably expressing nsp2 are referred to as DBT-nsp2, and the control cells that were stably transduced with vector only are referred to as DBT-vec.

Antibodies. Most of the rabbit polyclonal antibodies used in biochemical experiments have been previously described. For MHV, these include anti-nsp1 (VU221) (7), anti-nsp2 (VU154) (41), and anti-nsp8 (VU123) (5). For SARS-CoV, these include anti-nsp1 (VU231), anti-nsp2 (VU239), anti-nsp3 (VU 233), and anti-nsp8 (VU249) (37). These antibodies are further detailed in Table 1. The mouse monoclonal antibody directed against the structural protein nucleocapsid (anti-N, J3.3) was generously provided by John Fleming (University of Wisconsin, Madison).

Rabbit polyclonal antibodies against MHV nsp3 (VU164) were generated by Cocalico, Inc. (Reamstown, PA) using a recombinant nsp3 protein fragment as the antigen. All nsp3 nucleotide and amino acid numbers correspond to the MHV sequence reported before (2). Nucleotides 2709 to 3746 (ORF1 amino acids G_{833} to E_{1179}) corresponding to the N terminus of nsp3 were amplified by reverse transcription PCR using purified MHV genomic RNA as the template. Primer-generated restriction sites (5′ NcoI and 3′ XhoI) were used to subclone the PCR fragment into the pET23d bacterial expression vector (Novagen). A 38-kDa histidine-tagged protein was expressed in *Escherichia coli* BL21 cells, isolated using nickel resin chromatography according to the manufacturer's protocol, and further purified by SDS-PAGE and electroelution (Bio-Rad) as previously described (5).

Construction of mutant MHV and SARS-CoV infectious cDNA fragment A plasmids. Deletions of the nsp2 coding sequence were achieved for both viral infectious cDNAs using PCR and the primers shown in Table 2. For all primer sets, primers A and B generated an A/B PCR product, and primers C and D generated a C/D PCR product. For all MHV reactions, the MHV infectious cDNA fragment A construct (pCR-XL-TopoA), which consists of nucleotides 1 to 4882, was used as template DNA (52), and the coding region of nsp2 corresponds to nucleotides 951 to 2705 and amino acids Val248 to Ala832. For all SARS-CoV reactions, the SARS-CoV infectious cDNA fragment A construct (pSARS-icA), which consists of nucleotides 1 to 4419, was used as a template (51) and the coding region of nsp2 corresponds to nucleotides 805 to 2718 and amino acids Ala181 to Gly818. Mutant fragment A constructs for VURG 22 and VURG 23 were constructed using the class IIs restriction enzyme method (52) in which products A/B and C/D were ligated and cloned into the vector at unique 5′ SacII and 3′ NdeI sites. The mutant fragment A construct for SARSΔnsp2 was constructed by the class IIs restriction enzyme method and was cloned into the vector at unique 5′ BglII and 3′ NdeI sites. Successful deletions of the nsp2 coding sequences were confirmed by restriction digestion and sequencing.

Generation of MHV and SARS-CoV Δnsp2 mutant viruses. Viruses containing the PCR-generated deletion of the nsp2 coding sequence were produced using the infectious cDNA assembly strategies for MHV-A59 and SARS-CoV as previously described, with modifications (13, 43, 51, 52). Briefly, for MHV, plasmids containing the seven cDNA cassettes of the MHV genome were digested using MluI, BsmBI, and SfiI for fragment A, BglI and BsmBI for fragments B and C, BsmBI and NciI for fragments D and E, BsmBI for fragment F, and SfiI and BsmBI for fragment G. Digested, gel-purified fragments were ligated in a total reaction volume of ~170 μl overnight at 16°C. Following chloroform extraction and isopropanol precipitation of ligated DNA, capped, polyadenylated full-length RNA transcripts of MHV infectious cDNA were generated in vitro using the mMessage mMachine T7 transcription kit (Ambion) following the manufacturer's protocol with modifications. Fifty-microliter reactions were supplemented with 7.5 μl of 30 mM GTP, and transcription was performed at 40.5°C for 25 min, 37.5°C for 50 min, and 40.5°C for 25 min.

In parallel, capped, polyadenylated RNA transcripts encoding the MHV nucleocapsid protein (N) were generated in vitro using N cDNA generated from PCR (52). N transcripts and mutant MHV transcripts were then mixed and electroporated into BHK-MHVR cells. Briefly, BHK-MHVR cells were grown

TABLE 2. Primers used for generation of nsp2 deletion constructs

Primer	Sequence[a] (5′ → 3′)	Sense	Purpose
VURG22/23 A	$_{78}$AACGGCACTTCCTGCGTGTCCATG	+	PCR partner for MHV B primers
VURG22 B22	CGTCTCCTCTT$_{953}$AACACCGCGATAGCCCTTAAG	−	Mutagenesis for MHV VURG22
VURG22 C22	CGTCTCC$_{2709}$AAGAAAGTCGAGTTTAACGACAAGCC	+	Mutagenesis for MHV VURG22
VURG23 B23	CGTCTCCTGCC$_{953}$AACACCGCGATAGCCCTTAAG	−	Mutagenesis for MHV VURG23
VURG23 C23	CGTCTCC$_{2706}$GGCAAGAAAGTCGAGTTTAACGAC	+	Mutagenesis for MHV VURG23
VURG22/23 D	$_{3885}$ACTTGCACATATGAGACACAACGTCCCCA	−	PCR partner for MHV C primers
SARSΔnsp2 A	$_{30}$CCAACCAACCTCGATCTCTTGTAGATCTGTT	+	PCR partner for SARS B primers
SARSΔnsp2 B	GCTCTTCATGC$_{804}$ACCTCCATTGAGCTCACGAG	−	Mutagenesis for SARSΔnsp2
SARSΔnsp2 C	GCTCTTCAGCA$_{2722}$CCAATTAAAGGTGTAACCTTT	+	Mutagenesis for SARSΔnsp2
SARSΔnsp2 D	$_{3663}$ACCAAATATGCCTGCTGACAACAATGGTG	−	PCR partner for SARS C primers

[a] Underlined nucleotides incorporated for cloning or mutagenesis purposes. Nucleotide sequence position is indicated.

to subconfluence, trypsinized, then washed twice with phosphate-buffered saline (PBS) and resuspended in PBS at a concentration of 10^7 cells/ml. Six hundred microliters of cells was then added to RNA transcripts in a 4-mm gap electroporation cuvette (BTX), and three electrical pulses of 850 V at 25 μF were delivered with a Bio-Rad Gene Pulser Xcell electroporator. Transfected cells were then seeded onto a layer of 10^6 uninfected DBT cells in a 75-cm^2 flask and incubated at 37°C for 30 h.

For SARS-CoV, plasmids containing the six cDNA cassettes of the SARS-CoV genome were restriction-digested with MluI and BglI for fragment A, BglI for fragments B, C, D, and E, and BglI and NotI for fragment F. Digested fragments were then gel purified, ligated, and transcribed as above. SARS-CoV RNA and SARS-CoV N transcripts were then electroporated into 800 μl of 10^7 cells/ml Vero-E6 cells (450 V at 50 μF) and then seeded in a 75-cm^2 flask and incubated at 37°C for 72 h. Virus viability was determined by cytopathic effect (syncytium formation for MHV, cell rounding for SARS-CoV), and progeny were passaged and clones were isolated by plaque assay. RNA was recovered from infected cell monolayers from both MHV and SARS-CoV infections using TRIzol (Invitrogen) according to the manufacturer's instructions, and retention of introduced mutations was verified by reverse transcription-PCR and sequencing.

Viral growth assays. For viral growth determination, DBT cells were infected at a multiplicity of infection (MOI) of 5 PFU/cell with MHV, and Vero-E6 cells were infected at an MOI of 1 PFU/cell with SARS-CoV. Following a 45-minute adsorption with rocking at room temperature, medium was aspirated, and cells were washed three times with PBS and supplemented with warm medium. Cells were then incubated at 37°C. Aliquots of medium were collected from 1 to 24 h postinfection (p.i.), and virus titers were determined by plaque assay as described previously (27).

Protein immunoprecipitations and immunoblots. For protein labeling and immunoprecipitation experiments, cells were infected with MHV and incubated at 37°C. At 4.5 h p.i., medium was aspirated and replaced with medium lacking methionine and cysteine and supplemented with Actinomycin D (Sigma) at a final concentration of 20 μg/ml. At 6 h p.i., cells were labeled with [^{35}S]methionine/cysteine ([^{35}S]Met/Cys) at a concentration of 0.08 mCi/ml. Radiolabeled cells were lysed in 1 ml no-SDS lysis buffer (1% NP-40, 0.5% sodium deoxycholate, 150 mM sodium chloride, and 50 mM Tris, pH 8.0) at the indicated times p.i. Cellular debris and nuclei were pelleted by centrifugation at 1,500 × *g* for 5 min at 4°C, and the supernatant was transferred to a fresh tube. One hundred microliters of cell lysate was subsequently used per 1 ml of immunoprecipitation reaction buffer. Lysates that were boiled prior to immunoprecipitation were boiled for 5 min in SDS at a final concentration of 1%. The lysate was combined with protein A-Sepharose beads and a 1:200 dilution of antibody in no-SDS lysis buffer supplemented with 1% SDS. After incubation at 4°C for 4 h, beads were pelleted and washed with low-salt lysis buffer (no-SDS lysis buffer with 150 mM NaCl) followed by high-salt lysis buffer (no-SDS lysis buffer with 1 M NaCl) and a final low-salt wash. After rinsing, 30 ml of 2X SDS loading buffer (8% SDS, 0.2 M Tris, pH 8.8, 4 mM EDTA, 0.1% bromophenol blue, 40% glycerol, 0.5 M dithiothreitol) was added to the pelleted beads and boiled for 5 min prior to electrophoresis of the supernatant on 5 to 18% SDS-PAGE gels.

SARS-CoV-infected cells were lysed in buffer containing 20 mM Tris-HCl, pH 7.6, 150 mM NaCl, 0.5% sodium deoxycholate, 1% Nonidet P-40, and 0.1% SDS, and tested to confirm inactivation (11). Following centrifugation at 16,000 × *g* for 2 min to pellet nuclei, supernatants were treated with 1 volume of 10 mM EDTA/0.9% SDS. Lysates were then heated twice at 90°C for 30 min prior to use. Immunoblots to detect SARS-CoV proteins were then performed as described (37). Images were processed using Adobe Photoshop CS.

Metabolic labeling of viral RNA. For metabolic labeling of MHV viral RNA, DBT cell monolayers (~1.5×10^6 cells) were either mock infected or infected at an MOI of 5 PFU/cell. Virus was adsorbed for 30 min at room temperature. Medium was then aspirated and replaced with fresh, warm medium. Thirty minutes prior to labeling, actinomycin D was added to the cells at a final concentration of 20 μg/ml. Cells were labeled with 30 μCi [^{3}H]uridine in the presence of actinomycin D for the time intervals indicated. Cells were washed once with PBS and then lysed with 700 μl of no-SDS lysis buffer. Lysates were centrifuged at 1,500 × *g* to remove nuclei, and then RNA in 200 μl of cytosolic extract was precipitated using trichloroacetic acid. Precipitated RNA was dried onto glass microfiber filters (Whatman) using vacuum filtration, and radioactivity was measured in a liquid scintillation counter (Beckman). Quantitative analysis was performed using ImageJ (http://rsb.info.nih.gov/ij/).

Genomic and subgenomic RNA analysis by Northern blot. DBT cells (MHV) or Vero-E6 cells (SARS-CoV) were infected with wild-type or mutant viruses at an MOI of 5 PFU/cell (MHV) or 1 PFU/cell (SARS-CoV). RNA was harvested from cells at 10 h p.i. (MHV) or 12 h p.i. (SARS-CoV) in TRIzol (Invitrogen), isolated according to the manufacturer's instructions, and resuspended in formamide. RNA from approximately 1.7×10^5 cells was electrophoresed in a 0.6% agarose/2 M formaldehyde morpholinepropanesulfonic acid (MOPS) gel at 144 V for 4 h. RNA was then transferred to positively charged nylon membrane (Nytran, Schleicher and Schuell) by downward capillary transfer according to the manufacturer's instructions (TurboBlotter, Schleicher and Schuell). Blots were hybridized overnight at 42°C with 1.5 nM of the appropriate biotinylated deoxyoligonucleotide probe in ULTRAhyb-Oligo (Ambion).

Probes were designed to hybridize to a portion of the positive-sense 3′ untranslated region (UTR) of the respective viruses, and their sequences were 5′-CTGCAAGTCATCCATTCTGATAGAGAGTG-3′ for MHV (13, 49) and 5′-GGCTCTTTCAAGTCCTCCCTAATGTTAC-3′ for SARS-CoV. Probes were biotinylated with EZ-Link photoactivatable biotin (Pierce) according to the manufacturer's protocol. Following hybridization, probe signal was detected using the North2South detection kit (Pierce) according to the manufacturer's instructions. Images were processed using Adobe Photoshop CS. Quantitative analysis was performed using ImageJ (http://rsb.info.nih.gov/ij/).

Immunofluorescence detection of viral and stably expressed proteins. DBT cells or DBT-nsp2 cells grown to 60% confluence on 12-mm glass coverslips were infected with wild-type or mutant MHV at an MOI of 5 PFU/cell. At 6.5 h p.i., medium was aspirated from cells, and cells were fixed and permeabilized in −20°C methanol overnight. Cells were then rehydrated in PBS for 20 min, then blocked in PBS containing 5% bovine serum albumin. The following steps were performed in immunofluorescence assay wash solution (PBS containing 1% bovine serum albumin and 0.05% Nonidet P-40) at room temperature. Blocking solution was aspirated, and cells were incubated in primary antibody (anti-nsp2, 1:200, and anti-nucleocapsid [anti-N], 1:1,000) for 1 h. Cells were then washed in immunofluorescence assay wash solution three times for 10 min per wash. Cells were then incubated in secondary antibody (goat anti-rabbit-Alexa 488, 1:1,000, and goat anti-mouse-Alexa 546, 1:1,000, Molecular Probes) for 45 min. Cells were washed again three times for 10 min per wash, followed by a final wash in PBS, and then rinsed in distilled water. Coverslips were mounted with Aquapolymount (Polysciences) and visualized by confocal immunofluorescence microscopy on a Zeiss LSM 510 laser scanning confocal microscope at 488 and

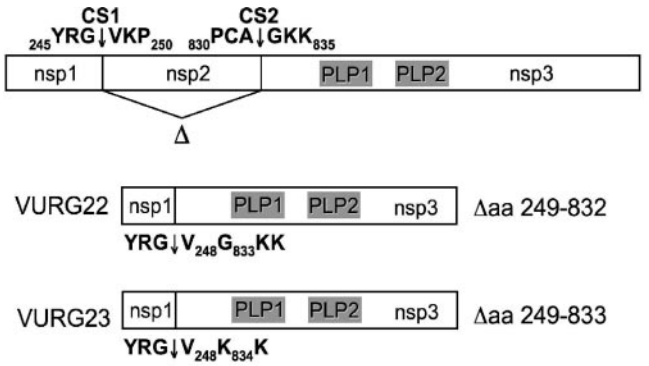

FIG. 2. Construction of MHVΔnsp2 viruses. (Top) The first three proteins of the replicase polyprotein, nsps 1 to 3, with amino acids at positions P3 to P3′ of the first two cleavage sites (CS1 and CS2) are shown. Cleavage positions are indicated by downward arrows, and amino acid residue numbers are indicated. (Middle and bottom) Because in vitro studies have not determined the minimal sequence required to allow PLP-mediated processing, deletions of nsp2 were achieved in two ways. Both deletions maintained the canonical CS1 P2-P1′ $_{246}$RG ↓ V_{248} to allow rapid processing of nsp1. (Middle) VURG22 was generated by deletion of amino acids Lys249 to Ala832 of nsp2, resulting in an nsp1/3 juxtaposition with unchanged nsp3 coding sequence directly fused to Val_{248}. (Bottom) VURG23 was generated by a deletion of the N-terminal amino acid Gly_{833} of wild-type nsp3 in addition to amino acids Lys249 to Ala832 of nsp2, so the nsp1/3 juxtaposition resulted in a cleavage site that more closely resembled that of CS1 P3 to P3′.

543 nm with a 40X oil immersion lens. Images were processed and assembled using Adobe Photoshop CS.

RESULTS

Generation and recovery of MHVΔnsp2 viruses. To determine whether the nsp2 domain is required for MHV replication, cloned genome fragments were engineered to delete the nsp2 coding sequence (Fig. 2). The nsp2 coding sequence is bounded by the nsp1-nsp2 cleavage site (cleavage site 1 [CS1] in this report) and the nsp2-nsp3 cleavage site (cleavage site 2 [CS2]). The P2 to P1′ residues of CS1 and CS2 are not identical in MHV. CS1 is composed of P2-ArgGly ↓ Val-P1′, while CS2 is composed of P2-CysAla ↓ Gly-P1′, and thus a direct juxtaposition of nsp1 and nsp3 would result in a chimeric nsp1/3 cleavage site, P2-ArgGly ↓ Gly-P1′. We therefore maintained the amino acid sequence corresponding to P2-P1′ of the CS1 cleavage site, incorporating the first amino acid of nsp2 to complete the cleavage site at P1′ (V_{248}), since in vitro and reverse genetic studies of cleavage at this site identified these residues as key determinants of cleavage (13, 15, 22).

Two different constructs were generated with different P2′ residues: VURG22 maintains the amino-terminal coding sequence of nsp3 ($_{833}$GKK) and VURG23 deletes the first Gly_{833} of nsp3, generating a P′ sequence that more closely resembles the native CS1. Mutated genome fragment A cDNAs were used to assemble in vitro full-length MHV genome cDNAs lacking the nsp2 coding sequence. The full-length cDNA was used to direct in vitro transcription of full-length genomic RNA, which was electroporated into BHK cells expressing the MHV receptor (BHK-MHVR cells) (13, 52). The electroporated cells were seeded onto subconfluent monolayers of DBT cells and monitored for cytopathic effect for 24 to 48 h.

Cells electroporated with the VURG22 and VURG23 genomes demonstrated a progressive cytopathic effect (syncytium formation) that began at 24 h postelectroporation and completely involved the seeded monolayer by 48 h postelectroporation. When clarified supernatant medium from the electroporated cells was used to infect fresh monolayers of DBT cells, >80% of cells were involved in syncytia by 12 h p.i., confirming the presence of infectious progeny virus. Total RNA was extracted from the infected monolayers and sequenced by reverse transcription-PCR from nucleotide 645 within the nsp1 coding region to nucleotide 3312 within the nsp3 coding region, confirming that the modified sequence with nsp2 deletion in recovered virus matched that introduced in the cDNA fragment (data not shown). No other nucleotide changes were identified in this region. Since the entire ~32-kb genome of recovered viruses was not sequenced, additional mutations outside of this region cannot be ruled out. Nevertheless, these results demonstrated that deletion of the nsp2 coding sequence from MHV allowed recovery of infectious virus and that no other mutations in the proteins flanking nsp2 were associated with recovery of virus.

Deletion of MHV nsp2 coding sequence results in wild-type growth kinetics but decreased virus titer. To determine the effect of nsp2 deletion on MHV growth, single-cycle growth assays were performed in which cell monolayers were infected with an MOI of 5 PFU/cell of wild-type recombinant virus (MHV-wtic) or the MHVΔnsp2 viruses VURG22 and VURG23. Samples of cell supernatant were harvested at time points from 1 to 24 h p.i., and viral titer was determined by plaque assay (Fig. 3). Infection with MHV-wtic virus resulted in peak titers of 6.7×10^7 PFU/ml at 12 h p.i. For VURG22 and VURG23, titers achieved at 12 h p.i. were ~0.5 $\log_{10}$ reduced for both mutants (1.2×10^7 PFU/ml peak for both viruses). These results demonstrate that deletion of nsp2 allows virus growth in cell culture with similar kinetics as wild-type virus and with only a modest reduction in peak titer. The growth curves of VURG22 and VURG23 were indistinguishable, demonstrating that the strategies resulting in different chimeric nsp1/3 cleavage sites yielded virus with similar growth fitness.

Polyprotein expression and processing in MHVΔnsp2 mutants. To determine the effects of nsp2 deletion on expression and processing of nsp1, nsp3, and the remainder of the replicase polyprotein, cytoplasmic lysates of cells infected with wild-type MHV and MHVΔnsp2 mutants were immunoprecipitated with antibodies against nsp1 (28 kDa), nsp2 (65 kDa), nsp3 (210 kDa), and the downstream, 3CLpro-processed nsp8 (22 kDa). To detect nsp3 produced in MHV-infected cells, a polyclonal antiserum was induced in rabbits against a recombinant protein polypeptide expressed in *E. coli* containing the amino-terminal 346 amino acids of nsp3 (amino acids G_{833} to E_{1179}). The anti-nsp3 antiserum (VU164) was first used to immunoprecipitate proteins from lysates of mock-infected or MHV-infected DBT cells (Fig. 4A). The anti-nsp3 antibodies detected a 210-kDa band in MHV-infected cells, which was not detected by immune serum in mock-infected cells or by preimmune serum from the same rabbit in virus-infected cells and which was consistent with the predicted mass of MHV nsp3.

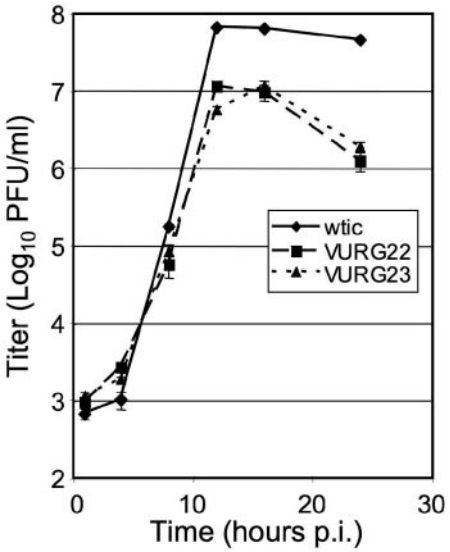

FIG. 3. Growth of MHVΔnsp2 viruses. DBT cells were infected with the indicated viruses at an MOI of 5. Samples of supernatant were taken at the indicated times postinfection, and titers were determined by plaque assay on DBT cells. wtic, recombinant wild-type control (MHV-wtic). A representative result from three experiments is shown. Error bars represent standard deviation across four replicate plaque assays within the experiment.

The immune anti-nsp3 antibodies also detected a protein of ~275 kDa in infected cells. The ~275-kDa protein was also detected when the cell lysate was boiled prior to immunoprecipitation with anti-nsp3, demonstrating that it was specifically recognized by anti-nsp3. The ~275-kDa protein was similar to high-molecular-weight proteins previously detected with other antibodies (12, 40), and had the mobility of a theoretical nsp2-nsp3 precursor. These results established the specificity of the anti-nsp3 antibody and showed it was capable of detecting both nsp3 and a higher-molecular-weight protein that was a putative nsp2-nsp3 precursor.

The anti-nsp3 antibodies were then used along with anti-nsp1, anti-nsp2, and anti-nsp8 to immunoprecipitate lysates from cells that were mock infected or infected with MHV-wtic or MHVΔnsp2 virus in the presence of [^{35}S]Met/Cys from 6 to 10 h p.i. (Fig. 4B). Both nsp2 and the putative nsp2-nsp3 precursor were detected in lysates from cells infected with MHV-wtic. As predicted from the sequences, neither nsp2 (65 kDa) nor the putative nsp2-nsp3 precursor (275 kDa) was detected in lysates from cells infected with MHVΔnsp2 viruses. In contrast, nsp1 (28 kDa), nsp3 (210 kDa), and nsp8 (22 kDa) all were detected at comparable levels in MHV-wtic-, VURG22-, and VURG23-infected cell lysates. Together, these experiments demonstrated that processing at the nsp3-nsp4 cleavage site was intact, as was the 3CLpro-mediated processing of nsp8. In addition, proteolytic processing at the engineered chimeric nsp1/3 cleavage sites of both MHVΔnsp2 mutants was complete, based on detection of distinct nsp1 and nsp3 bands and suggested by the lack of any detectable protein consistent with an uncleaved 238-kDa nsp1/3 precursor.

Since the P2′ residue of the chimeric nsp1/3 cleavage sites no longer matched the P2′ residue of wild-type CS1, these results demonstrated that the P2′ residue in the engineered chimeric

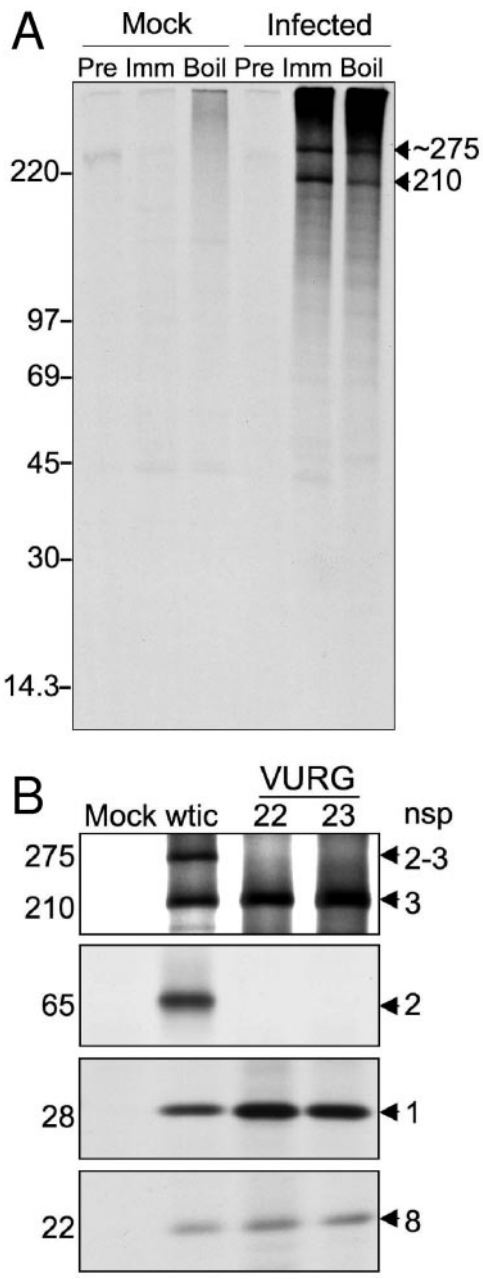

FIG. 4. Detection of MHV nsp3 and protein expression of MHVΔnsp2 viruses. (A) DBT cells were either mock infected or infected with MHV, and proteins were labeled with [^{35}S]Met/Cys from 6 to 8 h p.i. Following removal of nuclei by centrifugation, equal aliquots of cell lysate were then immunoprecipitated under the following conditions: using preimmune serum (pre); using anti-nsp3 antibodies (immune), or using anti-nsp3 antibodies following a 5-min boil in the presence of 1% SDS (boil). Proteins were then resolved by SDS-PAGE. Viral proteins are indicated to the right of the gel by mass in kDa. Molecular mass markers are shown to the left, with mass in kDa. (B) DBT cells were infected with the indicated viruses. Proteins were labeled with [^{35}S]Met/Cys from 6 to 10 h p.i. Cell lysates were immunoprecipitated with anti-nsp1, anti-nsp2, anti-nsp3, and anti-nsp8 antibodies, and proteins were resolved by SDS-PAGE. Proteins are indicated to the right of the gels by nsp number. Molecular mass, in kDa, is indicated to the left of the gels. nsp2–3 represents the precursor protein to nsp2 and nsp3 that is detectable in wild-type infections.

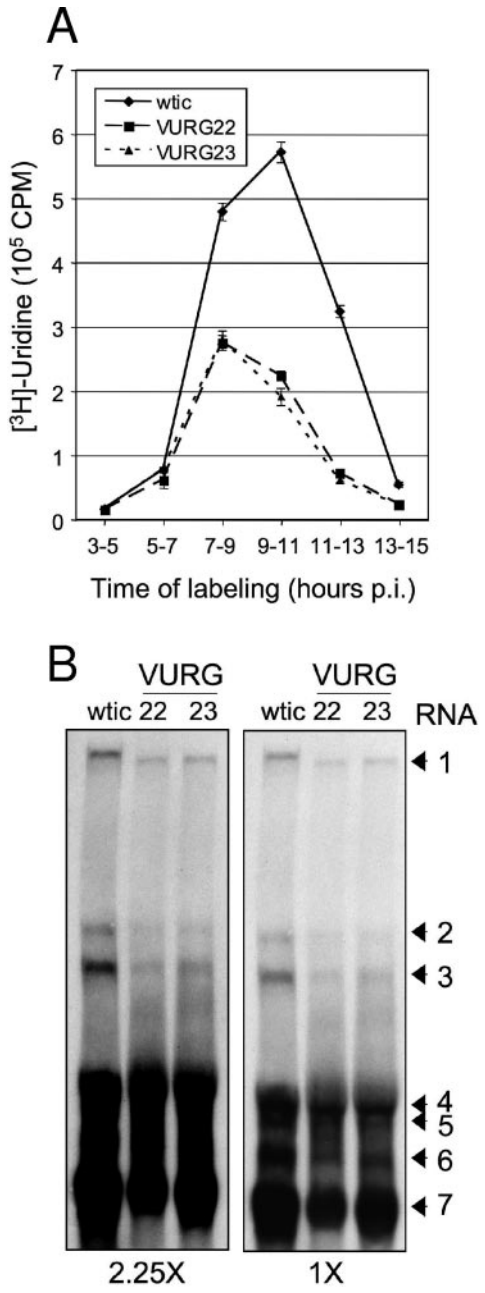

FIG. 5. RNA synthesis of MHVΔnsp2 viruses. (A) DBT cells in six-well plates were infected with the indicated viruses at an MOI of 5. Thirty minutes prior to labeling, medium was aspirated and replaced with warm medium containing actinomycin D. RNA was labeled with [^{3}H]uridine for the times indicated, cells were lysed, and [^{3}H]uridine incorporation was quantitated by scintillation counting of trichloroacetic acid-precipitable RNA. Error bars indicate standard deviation of triplicate trichloroacetic acid precipitations within one experiment. (B) DBT cells in 60-mm dishes were infected with the indicated viruses. Cells were lysed at 10 h p.i. in TRIzol, and RNA was isolated. RNA corresponding to 1.7×10^5 cells was electrophoresed in a 0.6% agarose–2 M formaldehyde–MOPS gel and transferred to a nylon membrane. Positive-stranded RNA species were hybridized with an antisense, biotinylated oligodeoxynucleotide probe that recognizes the 3′ UTR of MHV and visualized following detection by chemiluminescence. Relative exposure time is indicated below each blot, and RNA species are indicated to the right. RNA1 –genomic RNA. RNAs 2 to 7 –subgenomic RNAs.

nsp1/3 cleavage site did not abolish or inhibit the processing of nsp1 from nsp3. The results show that no specific amino acid sequences or other determinants in nsp2 are required for cleavage at either the nsp2 amino-terminal CS1 or carboxy-terminal CS2. Finally, the experiments provide the first direct genetic evidence from infectious virus that the ~275-kDa protein is the nsp2-nsp3 precursor.

MHVΔnsp2 mutant viruses have decreased RNA synthesis. To determine whether the growth defects of the MHVΔnsp2 mutants were associated with defects in viral RNA synthesis, cells infected at an MOI of 5 with MHV-wtic or the MHVΔnsp2 viruses were metabolically labeled with [^{3}H]uridine in the presence of actinomycin D for 2-h intervals from 3 to 15 h p.i. Total RNA was harvested in TRIzol and measured for trichloroacetic acid-precipitable incorporation of [^{3}H]uridine (Fig. 5A). The timing of peak incorporation of [^{3}H]uridine into mutant viral RNA was similar to that of MHV-wtic, occurring between 7 to 9 and 9 to 11 h p.i. However, when average total incorporation from 7 to 9 and 9 to 11 h was compared with MHV-wtic, RNA synthesis was reduced for both VURG22 (48% of MHV-wtic) and VURG23 (44% of MHV-wtic) (Fig. 5A).

To determine if changes in RNA synthesis were associated with species of RNA, monolayers of infected, nonradiolabeled cells were used to harvest RNA for Northern blot analysis of viral RNA species at 10 h p.i. (Fig. 5B). When total RNA was probed for positive-strand RNA, all genomic and subgenomic RNA species were detected. The only distinction between MHV-wtic and MHVΔnsp2 mutants was a decrease in the size of genome RNA, consistent with deletion of 5.6% of the genome (Fig. 5B). The mobility of other RNA species and the ratios of viral RNA1 to RNA7 for wild-type and mutant viruses (0.19 for MHV-wtic, 0.13 for VURG22, and 0.16 for VURG23) were not significantly different. Thus, the changes in viral RNA synthesis for the MHVΔnsp2 mutants reflected an overall reduction in RNA synthesis, but not a specific regulation or alteration of specific positive strand species.

MHVΔnsp2 viruses form replication complexes. MHV nsp2 previously has been shown to target to cytoplasmic replication complexes (6, 41), so we sought to determine if MHVΔnsp2 mutants demonstrated changes in the formation of replication complexes in the infected cell cytoplasm in the absence of nsp2. DBT cells on glass coverslips were infected with MHV-wtic or the MHVΔnsp2 viruses for 6.5 h, fixed, and probed by indirect immunofluorescence with anti-nsp2 and anti-N (nucleocapsid), since N localization is a marker for replication complexes at early times p.i. (Fig. 6A). DBT cells infected with wild-type virus demonstrated colocalization of nsp2 and N protein in discrete cytoplasmic foci, as previously described for MHV replication complexes. DBT cells that were infected with MHVΔnsp2 viruses had a pattern of N localization to punctate cytoplasmic complexes indistinguishable from that produced by wild-type virus, while no fluorescent signal was detected in VURG22- and VURG23-infected cells probed with anti-nsp2. Thus, the MHVΔnsp2 viruses are able to form replication complexes in the absence of nsp2 that are, by indirect immunofluorescence, identical to those of MHV-wtic-infected cells, indicating that nsp2 is not required for replication complex formation.

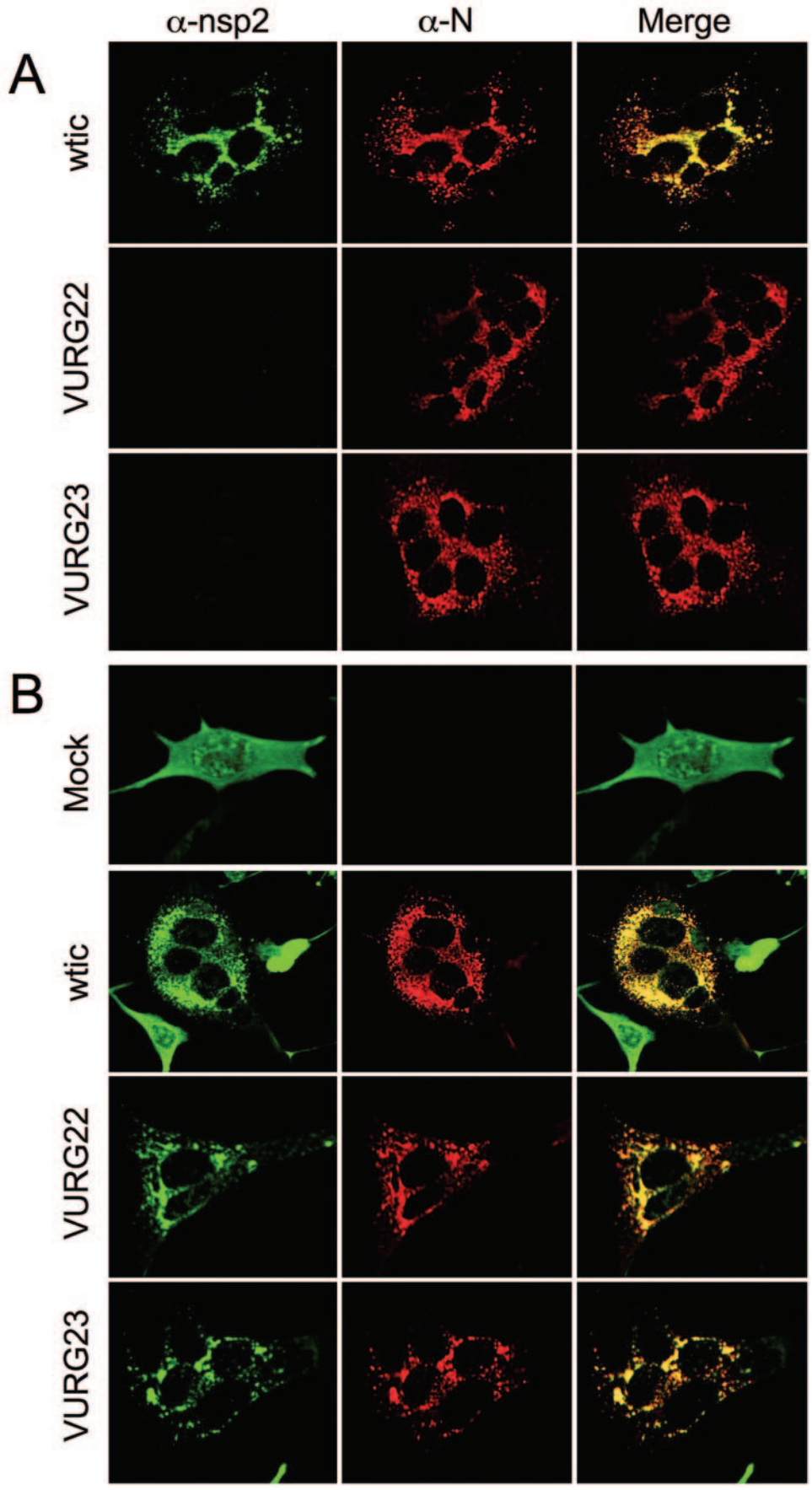
α-nsp2
α-N
Merge
A
wtic
VURG22
VURG23
B
Mock
wtic
VURG22
VURG23

Targeting of exogenous nsp2 to replication complexes of MHVΔnsp2 viruses. Since MHVΔnsp2 viruses were capable of forming replication complexes in the absence of nsp2 expression, we hypothesized that nsp2 may be targeted to replication complexes by other viral or virus-induced factors. Thus, we sought to determine whether exogenously expressed nsp2 was capable of trans targeting to replication complexes in the absence of viral nsp2. A system for exogenous expression of nsp2 was developed in which a retroviral construct that expressed nsp2 was generated (pBabe-nsp2). DBT cells were transduced and selected for stable expression of pBabe-nsp2 (DBT-nsp2 cells). Growth of DBT-nsp2 cells appeared identical to that of both nontransduced DBT cells and DBT cells transduced with the empty pBabe construct (data not shown).

To determine if exogenously expressed nsp2 was capable of *trans*-targeting to replication complexes in the absence of viral nsp2, DBT-nsp2 cells were infected with MHV-wtic or MHVΔnsp2 viruses. Cells were then analyzed by indirect immunofluorescence to determine the localization patterns of nsp2 and N. A diffuse distribution of nsp2 was observed in mock-infected DBT-nsp2 cells, with nsp2 protein detectable in the cytoplasm and to some extent in the nucleus of the stably expressing cells (Fig. 6B, top row). No nsp2 protein was detected in DBT cells transduced with the empty pBabe retroviral construct (DBT-vec cells, data not shown). When the DBT-nsp2 cells were infected with MHV-wtic, exogenously expressed nsp2 protein was detected exclusively colocalized with N in replication complexes (Fig. 6B, second row). In these cells, no nsp2 was found in the nucleus or diffuse in the cytoplasm, suggesting complete retargeting of expressed nsp2 to the replication complexes.

To determine if the recruitment of exogenous nsp2 to replication complexes required viral nsp2, DBT-nsp2 cells were infected with MHVΔnsp2 viruses. When cells were infected with MHVΔnsp2 viruses, the pattern of nsp2 colocalization with N in putative replication complexes was indistinguishable from that in MHV-wtic infection. These results demonstrate that exogenously expressed nsp2 does not target specific membranes in the absence of infection. However, exogenously expressed nsp2 can be recruited to and retained at replication complexes in *trans*. This recruitment does not require viral nsp2 but rather is mediated by interactions with other viral or virally induced proteins or RNAs. Finally, these results support the conclusion that the defect in viral growth and RNA synthesis observed in the nsp2 deletion viruses was not due to an inability of the viruses to form replication complexes.

Deletion of SARS-CoV nsp2 allows virus recovery, growth, nsp processing, and viral RNA synthesis. Although SARS-CoV encodes nsps 1, 2, and 3 that are most similar in organization and size to the MHV proteins, the observed differences between MHV and SARS-CoV in this region of their polyproteins made it difficult to predict whether deletion of SARS-CoV nsp2 would allow recovery of viable mutants phenotypically similar to MHVΔnsp2 mutants (Fig. 1) (37, 42). To determine whether the nsp2 domain of the SARS-CoV ORF1 polyprotein was required for viral replication, a construct of SARS-CoV cDNA fragment A was generated in which the SARS-CoV nsp2 coding sequence was deleted. Since the P2-P1′ residues of SARS-CoV CS1 and CS2 are identical, the SARS-CoV nsp1/3 juxtaposition was designed to generate a true chimeric cleavage site that maintained the native P5-P1 of nsp1 and the P1′-P5′ of nsp3 (Fig. 7A).

The SARS-CoV fragment A cDNA lacking the complete nsp2 coding sequence was used to assemble full-length cDNA of SARS-CoV, and in vitro-transcribed genomic RNA and N transcripts were electroporated into Vero-E6 cells. Cells demonstrated a progressive cell rounding cytopathic effect by 72 h postelectroporation, consistent with a productive cytopathic infection. RNA derived from plaque-purified virus was subjected to reverse transcription PCR, and sequence analysis of the region spanning nsp1 through nsp3 (nucleotides 604 to 3019) confirmed the deletion of nsp2 and generation of the intended chimeric nsp1/3 cleavage site, with no other mutations observed in this region (data not shown). This confirmed that deletion of the SARS-CoV nsp2 coding sequence allowed recovery of infectious virus.

The purified SARS Δnsp2 virus was analyzed for viral growth, protein processing, and RNA synthesis, as performed for MHVΔnsp2 viruses. Infection with SARS-Urbani and SARS-wtic (recombinant wild-type) virus resulted in titers of 3.6×10^7 PFU/ml and 5.5×10^7 PFU/ml, respectively, at 24 h p.i. (Fig. 7B). For SARSΔnsp2, titers achieved at 24 h p.i. were $\sim$1-$\log_{10}$ reduced (3.5×10^6 PFU/ml) compared to wild-type infections. These results demonstrate that, as for MHV, deletion of nsp2 of SARS-CoV allows virus growth in cultured cells with similar kinetics in comparison to wild-type viruses and with only a modest defect in titer.

To determine whether the decrease in titer observed for nsp2 deletion virus was associated with alterations in processing at the chimeric nsp1/3 cleavage site or at other cleavage sites in the polyprotein, mock-infected and infected cell lysates were analyzed by immunoblot for viral proteins using anti-SARS nsp1, anti-SARS nsp2, anti-SARS nsp3, and anti-SARS nsp8 antibodies (Fig. 7C) (37). nsp2 was readily detected during SARS-wtic infection but was absent from cells infected with SARSΔnsp2. In contrast, nsp1, nsp3, and nsp8 were detected as mature processed proteins in both SARS-CoV- and SARSΔnsp2-infected cells. These experiments confirmed the absence of nsp2 protein in SARSΔnsp2-infected cell lysates and the normal processing of nsp3 by papain-like protease and of nsp8 by 3CLpro. Thus, the growth defect in SARSΔnsp2 was not due to inactivation of proteinases or abrogation of polypro-

FIG. 6. Replication complex formation in MHVΔnsp2-infected cells. (A) DBT cells on glass coverslips were infected with the indicated viruses. At 6.5 h p.i., cells were fixed and permeabilized in −20°C methanol, rehydrated in PBS, and analyzed by indirect immunofluorescence using anti-nsp2 (green) and anti-N (red). Yellow pixels represent colocalization as evidenced by overlapping green and red pixels. Cells were imaged on a Zeiss LSM 510 confocal microscope at 40X magnification. (B) DBT-nsp2 cells (see Materials and Methods) were infected, fixed, stained, and analyzed by indirect immunofluorescence as in A. Mock cells were mock infected and then treated identically to infected cells. N –nucleocapsid protein, a marker for replication complexes.

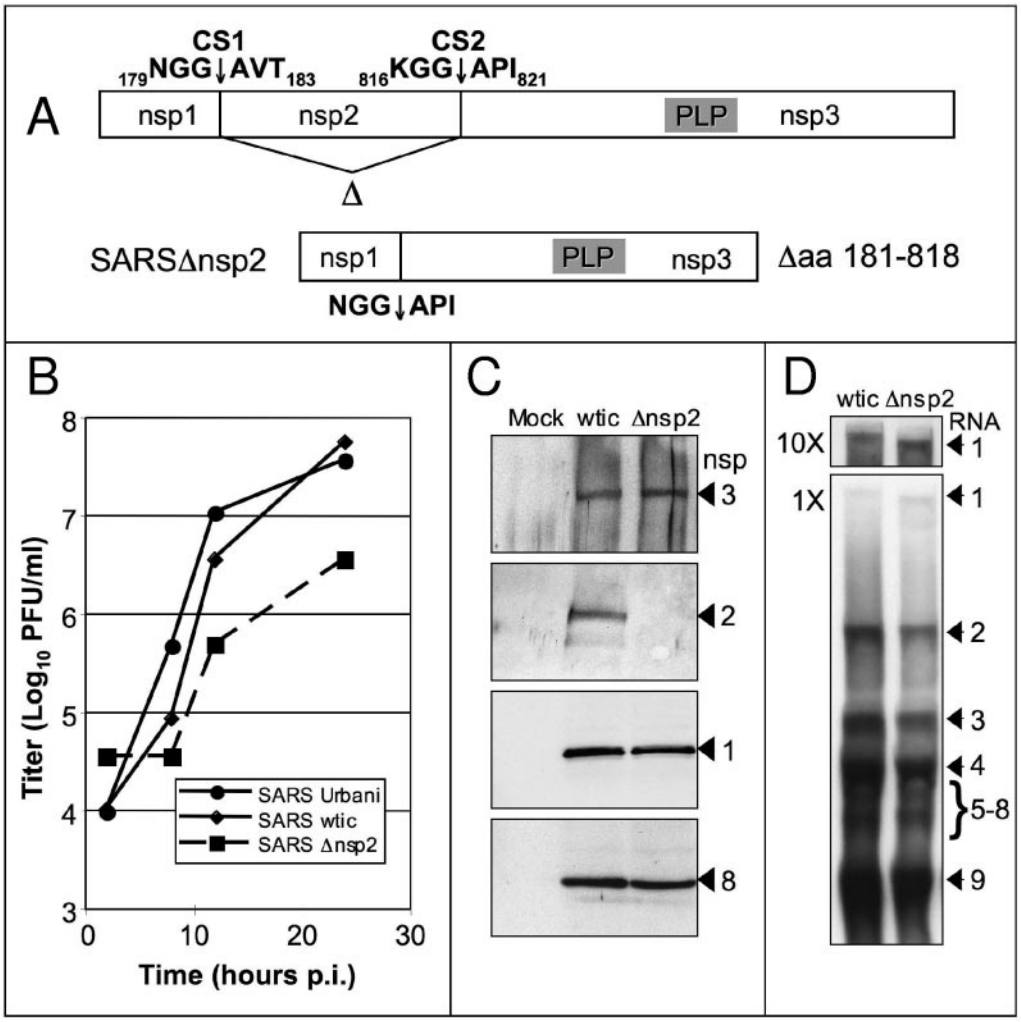

FIG. 7. Construction and characterization of SARS-CoVΔnsp2 virus. (A) The first three proteins of the replicase polyprotein, nsps 1 to 3, with amino acids at positions P3 to P3′ of the first two cleavage sites (CS1 and CS2) are shown. Cleavage positions are indicated by downward arrows, and amino acid residue numbers are indicated. The deletion of SARS-CoV nsp2 was achieved by deleting amino acids Ala181 to Gly818 of the nsp2 coding sequence, generating an nsp1/3 juxtaposition. (B) Growth of SARS-CoV nsp2 deletion virus. Vero-E6 cells were infected at an MOI of 1 with the indicated viruses. Samples of supernatant were taken at the indicated times postinfection, and titers were determined by plaque assay on Vero-E6 cells. SARS Urbani –parent wild-type strain to recombinant SARS-CoV. SARS wtic –recombinant wild-type SARS-CoV control. (C) Protein expression of SARS-CoV nsp2 deletion virus. Vero-E6 cells were infected with the indicated viruses and harvested at 12 h p.i. Viral proteins were resolved by SDS-PAGE and detected by immunoblot using SARS-CoV anti-nsp1, anti-nsp2, anti-nsp3, and anti-nsp8 antibodies. Proteins are indicated to the right of the gels by nsp number. (D) Accumulation of genomic and subgenomic RNAs of SARS-CoV nsp2 deletion virus. Vero-E6 cells in 60-mm dishes were infected with the indicated viruses. Cells were lysed at 12 h p.i. in TRIzol, and RNA was isolated. RNA corresponding to 1.7×10^5 cells was electrophoresed in a 0.6% agarose/2 M formaldehyde/MOPS gel and transferred to a nylon membrane. Positive-stranded RNA species were hybridized with an antisense, biotinylated oligodeoxynucleotide probe complementary to the 3′ UTR and detected by chemiluminescence. Relative exposure time is indicated to the left of each blot, and RNA species are indicated to the right. RNA1 –genomic RNA. RNAs 2 to 9 –subgenomic RNAs.

tein processing events. These experiments also extended the observations with the MHVΔnsp2 mutant viruses, demonstrating that a chimeric cleavage site generated by direct juxtaposition of nsp1 and nsp3 coding sequences with no altered or additional residues can be recognized and cleaved by PLP.

To determine whether the growth defect observed in SARSΔnsp2 was due to a defect in the accumulation of any particular positive-strand species of viral RNA, Northern blot analysis was performed on RNA extracted from SARS-wtic- or SARSΔnsp2-infected Vero-E6 cells using an antisense probe complementary to the 3′ UTR to detect all positive-strand RNA species (Fig. 7D). The SARSΔnsp2 virus produced all genomic and subgenomic RNAs, and the ratios of RNA1 to RNA9 were comparable to SARS-wtic (0.34 for SARS-wtic and 0.28 for SARSΔnsp2). Likewise, a change in electrophoretic mobility was observed for genomic RNA (RNA1) of SARSΔnsp2, consistent with the calculated 6.4% reduction in the size of RNA1 of SARSΔnsp2. These results demonstrate

that deletion of the nsp2 coding sequence of SARS-CoV does not result in a defect in the production of any particular positive strand viral RNA species.

DISCUSSION

In this study, we have demonstrated that the nsp2 protein domain is dispensable for MHV and SARS-CoV replication in cell culture. We have not identified any published report of the deletion of a complete mature protein domain from the polyprotein of a positive-stranded RNA virus that allowed autonomous replication. Deletions within polyproteins of western equine encephalitis virus, infectious bovine diarrhea virus, Moloney sarcoma virus, and others, for instance, have been reported, but these have not resulted in loss of complete mature protein domains (31, 35, 48). Whether complete deletions with autonomous replication have not been attempted or have been unsuccessful cannot be ascertained from the lack of reports. However, requirements for the maintenance of RNA structure, RNA replication, protein translation, polyprotein processing, and protein function have been presumed to impose formidable restrictions on the deletion of mature protein domains from polyproteins.

The viability and replication competency of the MHV and SARS-CoV nsp2 deletion mutants argue that, at least for coronaviruses, the above theoretical assumptions need to be reconsidered. The deletion of the nsp2 domain of the MHV and SARS-CoV replicase polyproteins was tolerated with only modest growth and RNA defects and no detectable effect on polyprotein processing in the recovered mutant viruses. The experimental results clearly indicate that neither the nsp2 proteins nor the RNA genome sequences encoding nsp2 are required for generation of infectious virus in cell culture. The results also demonstrate that the translation and processing of the ORF1 polyprotein, intermediate precursors, and mature proteins can occur in the setting of a major engineered deletion of the polyprotein coding sequence.

Whether the coronaviruses are a special case or reflect a previously uncharacterized "plasticity" within positive-stranded RNA viruses that express mature proteins from polyproteins, we can conclude that there may be significantly greater flexibility in the polyprotein organization, translation, and processing than had been assumed prior to this study. In addition, the experimental results raise important questions as to possible novel functions of "replicase gene" proteins during virus infection as well as conservation of functions between coronaviruses for proteins that have limited amino acid similarity.

Processing of nsp1, nsp2, and nsp3 precursors and mature proteins. The delayed cleavage of MHV nsp2 (p65) from a >240-kDa intermediate processed precursor was first reported in 1995 (12), and subsequent metabolic labeling and protein processing studies strongly supported a relationship between a 240- to 290-kDa protein and nsp2 and nsp3 (18, 40). The present study allowed direct comparison of precursors and mature proteins from viruses containing and lacking nsp2. The detection of nsp2 (p65) and the 275-kDa protein in MHV-wtic but complete absence of these proteins in the MHVΔnsp2 mutants provides direct genetic confirmation that the 275-kDa protein is an nsp2-nsp3 precursor. Simultaneously, the same experiments conclusively show that the nsp2-nsp3 precursor is not required either for nsp3 expression, PLP-mediated proteolysis, or virus replication in culture. Recently, an nsp2-nsp3 precursor was reported for SARS-CoV (19). The viability of the SARS-CoVΔnsp2 mutant similarly demonstrates that the SARS-CoV nsp2-nsp3 precursor is not required for growth in culture.

Our recent study involving MHV nsp2 processing addressed the determinants of processing at the N-terminal cleavage site of nsp2, the nsp1-nsp2 cleavage site (CS1) (13). While we demonstrated in that study that processing determinants at residues P5 through P5′ of CS1 during viral replication conformed to those identified in in vitro studies (3, 15), this study further demonstrates that a chimeric cleavage site, possessing amino acid residues from the C terminus of nsp1 and the N terminus of nsp3, was processed, showing that the context of the cleavage sites can be dramatically altered and still be recognized and cleaved. Whereas SARS-CoV P2-P1′ residues are identical for the nsp1-nsp2 and nsp2-nsp3 cleavage sites, this is not the case for MHV. The residues occupying the P2-P1′ sites of the cleavage sites are RG↓V for nsp1-nsp2 (CS1) and CA↓G for nsp2-nsp3 (CS2). The chimeras generated in this study did not assess the effect of directly fusing the C terminus of MHV nsp1 to the N terminus of nsp3, instead incorporating the N-terminal amino acid residue of nsp2, Val_{248}, to preserve the CS1 P2-P1′ context.

In spite of this, however, the processing of both SARS-CoV and MHV nsp1 from nsp3 observed in this study argues that one of two circumstances may be required to allow PLP-mediated processing. The first possibility is that only the proximal residues of the cleavage site are required for processing. In vitro studies identified optimal residues from P6 to P2′ for processing (4, 15, 22) and our results in this study suggest that the identity of the P1′ residue is not critical. However, another in vitro study suggests that a substrate of at least 69 kDa must be present for efficient PLP1-mediated processing to occur (45). Thus, another possibility is that, provided the cleavage site is accessible to the proteinase, a major factor determining whether or not cleavage will occur at these sites is the presence of a suitable upstream amino acid sequence context (context A) and a suitable downstream amino acid sequence context (context B). This hypothesis argues that, assuming sufficient contexts A and B are present, functional cleavage site chimeras can be generated.

The observed kinetics of nsp 1, 2, and 3 processing in wild-type infection would suggest that context plays a role in the availability of cleavage sites and efficiency of processing. This model would predict that the deletion of nsp2 and juxtaposition of nsp1 and nsp3 creates a new combination of proximal cleavage site determinants and contexts A and B that result in efficient cleavage at the chimeric site. Finally, our previous study with engineered CS1 cleavage mutants and this study suggest that amino acid residues in context A may play a more important role in proteolytic recognition and/or processing than amino acid residues in context B for PLP-mediated polyprotein processing (13). This suggests the possibility that only cleavage site and context determinants in the "upstream" protein are required for recognition and cleavage by the proteinase in the setting of viral infection. These hypotheses will be tested by altering the A and B contexts, such as by inserting a foreign gene with and without proximal cleavage site context

and testing for cleavage efficiency. Expression of foreign genes by insertion between the nsp1 and nsp2 coding sequences of a coronavirus replicon system has been shown for human coronavirus 229E, though effects on ORF1 protein expression and proteolytic processing were not directly assessed (20).

MHV and SARS-CoV nsp2 proteins: distinct sequences with similar functions? Though SARS-CoV differs in many ways from other coronaviruses studied to date, it has been stated that in ORF1, it is most similar to the group 2 coronaviruses (42). Following the pattern of all other coronaviruses, nsps 1 to 3 of SARS-CoV are the most variable compared with those of MHV and other coronaviruses, suggesting the possibilities of positive selective pressure and evolution of virus-specific functions. However, the observations that both MHV and SARS-CoV tolerate deletion of nsp2 and that these deletion viruses display remarkably similar phenotypes in growth, RNA synthesis, and protein processing suggest that the nsp2 proteins of MHV and SARS-CoV may serve similar functions in replication, or possibly in virus-cell interactions or pathogenesis.

The delayed cleavage of nsp2 from nsp3, the exclusive localization to replication complexes, and the growth and RNA defects of the nsp2 deletion mutants all argue that nsp2 may be serving roles in regulation of global RNA synthesis that, while not essential, serve to optimize generation of infectious virus. While a 50% decrease in RNA synthesis and a 1-$\log_{10}$ reduction in growth may allow propagation in culture, such a "modest" defect might significantly attenuate or abolish replication or virulence during infection of animals. Testing of the MHV and SARS-CoV nsp2 deletion mutants in different cell types and directly in animals for replication and virulence will be necessary to test these possibilities.

While we propose that the similar phenotypic changes in MHV and SARS-CoV nsp2 deletion mutants are due to lack of expression of nsp2 and nsp2-nsp3, we cannot exclude the possibility that the changes are due to the deletion of >5% of the viral genomes, with possible effects on RNA synthesis and growth. The extensive differences in SARS-CoV and MHV RNA in the nsp2 coding region, along with the lack of predicted secondary structures, argues against an RNA defect being responsible for the observed changes. Unambiguous demonstration that the observed replication and RNA synthesis defects are due to loss of nsp2 or the nsp2-nsp3 precursor will require complementation of the deficits by exogenously expressed proteins.

In this study, we demonstrated that nsp2 stably expressed in DBT cells by retroviral transduction was able to target to the replication complexes of MHV mutants lacking nsp2 expression. However, DBT-nsp2 cells generated in this study exhibited a broad range of expression levels of nsp2, but not all cells were infected during high-MOI infections. Thus, only 5 to 10% of DBT-nsp2 cells both expressed nsp2 and demonstrated detectable infection. Because of this, we concluded that the modest growth and RNA defects of the MHVΔnsp2 mutants could not be directly tested for complementation in this system. Such studies may require more highly impaired mutants, cells selected for specific levels of protein expression, or alternative methods of nsp2 expression, such as replicons or heterologous viruses.

In conclusion, we have engineered and established mutant MHV and SARS-CoV viruses containing deletions of the nsp2 coding sequence. These viruses did not produce the nsp2 protein, yet processed other replicase proteins correctly and replicated well in cell culture. These observations demonstrate for the first time that for the coronaviruses, at least one mature ORF1 protein domain is dispensable for replication in cell culture. Furthermore, these results bring to light a previously uncharacterized flexibility for deletion and reorganization within the coronavirus replicase polyprotein, providing insights into the requirements for the formation and function of the coronavirus replication complex. Finally, these findings will form the basis for studies of replicase protein involvement in host pathogenesis, virus-cell interactions, and virus complementation and new approaches to the development of stably attenuated animal and human coronaviruses.

ACKNOWLEDGMENTS

We thank Xiao Tao Lu, Christopher Aiken, Jing Zhou, and Kristen Guglielmi for technical assistance. We also thank Sadie Coberley, Elizabeth Eby, Lance Eckerle, Jeanne Malloy, and Jennifer Sparks for critical readings of the manuscript.

Support for this work was provided by National Institutes of Health grants RO1 AI26603 (M.R.D.), RO1 AI059136-01 (R.S.B.), and PO1 AI059443-01 (R.S.B. and M.R.D.) and Training Grant 5T32GM00855 for Cellular, Biochemical, and Molecular Sciences, Vanderbilt University School of Medicine (R.L.G.). Additional support was provided by Public Health Service award CA68485 for the Vanderbilt DNA Sequencing Shared Resource and the Molecular Imaging Shared Resource of the Vanderbilt-Ingram Cancer Center.

REFERENCES

1. **Baker, S. C., K. Yokomori, S. Dong, R. Carlisle, A. E. Gorbalenya, E. V. Koonin, and M. M. Lai.** 1993. Identification of the catalytic sites of a papain-like cysteine proteinase of murine coronavirus. J. Virol. **67:**6056–6063.
2. **Bonilla, P. J., A. E. Gorbalenya, and S. R. Weiss.** 1994. Mouse hepatitis virus strain A59 RNA polymerase gene ORF 1a: heterogeneity among MHV strains. Virology **198:**736–740.
3. **Bonilla, P. J., S. A. Hughes, J. D. Pinon, and S. R. Weiss.** 1995. Characterization of the leader papain-like proteinase of MHV-A59: identification of a new in vitro cleavage site. Virology **209:**489–497.
4. **Bonilla, P. J., S. A. Hughes, and S. R. Weiss.** 1997. Characterization of a second cleavage site and demonstration of activity in *trans* by the papain-like proteinase of the murine coronavirus mouse hepatitis virus strain A59. J. Virol. **71:**900–909.
5. **Bost, A. G., R. H. Carnahan, X. T. Lu, and M. R. Denison.** 2000. Four proteins processed from the replicase gene polyprotein of mouse hepatitis virus colocalize in the cell periphery and adjacent to sites of virion assembly. J. Virol. **74:**3379–3387.
6. **Bost, A. G., E. Prentice, and M. R. Denison.** 2001. Mouse hepatitis virus replicase protein complexes are translocated to sitesof M protein accumulation in the ERGIC at late times of infection. Virology **285:**21–29.
7. **Brockway, S. M., X. T. Lu, T. R. Peters, T. S. Dermody, and M. R. Denison.** 2004. Intracellular localization and protein interactions of the gene 1 protein p28 during mouse hepatitis virus replication. J. Virol. **78:**11551–11562.
8. **Chen, C., and H. Okayama.** 1987. High-efficiency transformation of mammalian cells by plasmid DNA. Mol. Cell. Biol. **7:**2745–2752.
9. **Chen, W., and R. S. Baric.** 1996. Molecular anatomy of mouse hepatitis virus persistence: coevolution of increased host cell resistance and virus virulence. J. Virol. **70:**3947–3960.
10. **Chen, W., V. J. Madden, C. J. Bagnell, and R. S. Baric.** 1997. Host-derived intracellular immunization against mouse hepatitis virus infection. Virology **228:**318–332.
11. **Darnell, M. E., K. Subbarao, S. M. Feinstone, and D. R. Taylor.** 2004. Inactivation of the coronavirus that induces severe acute respiratory syndrome, SARS-CoV. J. Virol. Methods **121:**85–91.
12. **Denison, M. R., S. A. Hughes, and S. R. Weiss.** 1995. Identification and characterization of a 65-kDa protein processed from the gene 1 polyprotein of the murine coronavirus MHV-A59. Virology **207:**316–320.
13. **Denison, M. R., B. Yount, S. M. Brockway, R. L. Graham, A. C. Sims, X. Lu, and R. S. Baric.** 2004. Cleavage between replicase proteins p28 and p65 of mouse hepatitis virus is not required for virus replication. J. Virol. **78:**5957–5965.
14. **de Vries, A. A. F., M. C. Horzinek, P. J. M. Rottier, and R. J. deGroot.** 1997. The genome organisation of the nidovirales: similarities and differences between arteri-, toro-, and coronaviruses. Semin. Virology **8:**33–47.

15. **Dong, S., and S. C. Baker.** 1994. Determinants of the p28 cleavage site recognized by the first papain-like cysteine proteinase of murine coronavirus. Virology **204:**541–549.
16. **Forsell, K., M. Suomalainen, and H. Garoff.** 1995. Structure-function relation of the NH2-terminal domain of the Semliki Forest virus capsid protein. J. Virol. **69:**1556–1563.
17. **Gorbalenya, A. E., E. V. Koonin, A. P. Donchenko, and V. M. Blinov.** 1989. Coronavirus genome: prediction of putative functional domains in the nonstructural polyprotein by comparative amino acid sequence analysis. Nucleic Acids Res. **17:**4847–4861.
18. **Gosert, R., A. Kanjanahaluethai, D. Egger, K. Bienz, and S. C. Baker.** 2002. RNA replication of mouse hepatitis virus takes place at double-membrane vesicles. J. Virol. **76:**3697–3708.
19. **Harcourt, B. H., D. Jukneliene, A. Kanjanahaluethai, J. Bechill, K. M. Severson, C. M. Smith, P. A. Rota, and S. C. Baker.** 2004. Identification of severe acute respiratory syndrome coronavirus replicase products and characterization of papain-like protease activity. J. Virol. **78:**13600–13612.
20. **Hertzig, T., E. Scandella, B. Schelle, J. Ziebuhr, S. G. Siddell, B. Ludewig, and V. Thiel.** 2004. Rapid identification of coronavirus replicase inhibitors using a selectable replicon RNA. J. Gen. Virol. **85:**1717–1725.
21. **Hirano, N., K. Fujiwara, and M. Matumoto.** 1976. Mouse hepatitis virus (MHV-2); plaque assay and propagation in mouse cell line DBT cells. Jpn. J. Microbiol. **20:**219–225.
22. **Hughes, S. A., P. J. Bonilla, and S. R. Weiss.** 1995. Identification of the murine coronavirus p28 cleavage site. J. Virol. **69:**809–813.
23. **Ivanov, K. A., T. Hertzig, M. Rozanov, S. Bayer, V. Thiel, A. E. Gorbalenya, and J. Ziebuhr.** 2004. Major genetic marker of nidoviruses encodes a replicative endoribonuclease. Proc. Natl. Acad. Sci. USA **101:**12694–12699.
24. **Ivanov, K. A., V. Thiel, J. C. Dobbe, Y. van der Meer, E. J. Snijder, and J. Ziebuhr.** 2004. Multiple enzymatic activities associated with severe acute respiratory syndrome coronavirus helicase. J. Virol. **78:**5619–5632.
25. **Kanjanahaluethai, A., and S. C. Baker.** 2000. Identification of mouse hepatitis virus papain-like proteinase 2 activity. J. Virol. **74:**7911–7921.
26. **Khromykh, A. A., M. T. Kenney, and E. G. Westaway.** 1998. trans-Complementation of flavivirus RNA polymerase gene NS5 by using Kunjin virus replicon-expressing BHK cells. J. Virol. **72:**7270–7279.
27. **Kim, J. C., R. A. Spence, P. F. Currier, X. T. Lu, and M. R. Denison.** 1995. Coronavirus protein processing and RNA synthesis is inhibited by the cysteine proteinase inhibitor e64dd. Virology **208:**1–8.
28. **Koonin, E. V.** 1991. The phylogeny of RNA-dependent RNA polymerases of positive-strand RNA viruses. J Gen. Virol. **72:**2197–2206.
29. **Liljestrom, P., S. Lusa, D. Huylebroeck, and H. Garoff.** 1991. In vitro mutagenesis of a full-length cDNA clone of Semliki Forest virus: the small 6,000-molecular-weight membrane protein modulates virus release. J. Virol. **65:**4107–4113.
30. **Lu, Y., X. Lu, and M. R. Denison.** 1995. Identification and characterization of a serine-like proteinase of the murine coronavirus MHV-A59. J. Virol. **69:**3554–3559.
31. **Mendez, E., N. Ruggli, M. S. Collett, and C. M. Rice.** 1998. Infectious bovine viral diarrhea virus (strain NADL) RNA from stable cDNA clones: a cellular insert determines NS3 production and viral cytopathogenicity. J. Virol. **72:**4737–4745.
32. **Meyers, G., A. Saalmuller, and M. Buttner.** 1999. Mutations abrogating the RNase activity in glycoprotein E(rns) of the pestivirus classical swine fever virus lead to virus attenuation. J. Virol. **73:**10224–10235.
33. **Morgenstern, J. P., and H. Land.** 1990. Advanced mammalian gene transfer: high titre retroviral vectors with multiple drug selection markers and a complementary helper-free packaging cell line. Nucleic Acids Res. **18:** 3587–3596.
34. **Myles, K. M., D. J. Pierro, and K. E. Olson.** 2003. Deletions in the putative cell receptor-binding domain of Sindbis virus strain MRE16 E2 glycoprotein reduce midgut infectivity in *Aedes aegypti*. J. Virol. **77:**8872–8881.
35. **Oskarsson, M. K., J. H. Elder, J. W. Gautsch, R. A. Lerner, and G. F. Vande Woude.** 1978. Chemical determination of the m1 Moloney sarcoma virus pP60gag gene order: evidence for unique peptides in the carboxy terminus of the polyprotein. Proc. Natl. Acad. Sci. USA **75:**4694–4698.
36. **Prentice, E., W. G. Jerome, T. Yoshimori, N. Mizushima, and M. R. Denison.** 2004. Coronavirus replication complex formation utilizes components of cellular autophagy. J. Biol. Chem. **279:**10136–10141.
37. **Prentice, E., J. McAuliffe, X. Lu, K. Subbarao, and M. R. Denison.** 2004. Identification and characterization of severe acute respiratory syndrome coronavirus replicase proteins. J. Virol. **78:**9977–9986.
38. **Sasaki, J., S. Nagashima, and K. Taniguchi.** 2003. Aichi virus leader protein is involved in viral RNA replication and encapsidation. J. Virol. **77:**10799–10807.
39. **Scarselli, E., H. Ansuini, R. Cerino, R. M. Roccasecca, S. Acali, G. Filocamo, C. Traboni, A. Nicosia, R. Cortese, and A. Vitelli.** 2002. The human scavenger receptor class B type I is a novel candidate receptor for the hepatitis C virus. EMBO J. **21:**5017–5025.
40. **Schiller, J. J., A. Kanjanahaluethai, and S. C. Baker.** 1998. Processing of the coronavirus mhv-jhm polymerase polyprotein: identification of precursors and proteolytic products spanning 400 kilodaltons of ORF1a. Virology **242:**288–302.
41. **Sims, A. C., J. Ostermann, and M. R. Denison.** 2000. Mouse hepatitis virus replicase proteins associate with two distinct populations of intracellular membranes. J. Virol. **74:**5647–5654.
42. **Snijder, E. J., P. J. Bredenbeek, J. C. Dobbe, V. Thiel, J. Ziebuhr, L. L. Poon, Y. Guan, M. Rozanov, W. J. Spaan, and A. E. Gorbalenya.** 2003. Unique and conserved features of genome and proteome of SARS-coronavirus, an early split-off from the coronavirus group 2 lineage. J. Mol. Biol. **331:**991–1004.
43. **Sperry, S. M., L. Kazi, R. L. Graham, R. S. Baric, S. R. Weiss, and M. R. Denison.** 2005. Single-amino-acid substitutions in open reading frame (ORF) 1b-nsp14 and ORF 2a proteins of the coronavirus mouse hepatitis virus are attenuating in mice. J. Virol. **79:**3391–3400.
44. **Suzuki, N., B. Chen, and D. L. Nuss.** 1999. Mapping of a hypovirus p29 protease symptom determinant domain with sequence similarity to potyvirus HC-Pro protease. J. Virol. **73:**9478–9484.
45. **Teng, H., J. D. Pinon, and S. R. Weiss.** 1999. Expression of murine coronavirus recombinant papain-like proteinase: efficient cleavage is dependent on the lengths of both the substrate and the proteinase polypeptides. J. Virol. **73:**2658–2666.
46. **Thiel, V., K. A. Ivanov, A. Putics, T. Hertzig, B. Schelle, S. Bayer, B. Weissbrich, E. J. Snijder, H. Rabenau, H. W. Doerr, A. E. Gorbalenya, and J. Ziebuhr.** 2003. Mechanisms and enzymes involved in SARS coronavirus genome expression. J. Gen. Virol. **84:**2305–2315.
47. **Thiel, V., and S. G. Siddell.** 2005. Reverse genetics of coronaviruses using vaccinia virus vectors. Curr. Top. Microbiol. Immunol. **287:**199–227.
48. **Turell, M. J., M. L. O'Guinn, and M. D. Parker.** 2003. Limited potential for mosquito transmission of genetically engineered, live-attenuated western equine encephalitis virus vaccine candidates. Am. J. Trop. Med. Hyg. **68:**218–221.
49. **Wu, H. Y., J. S. Guy, D. Yoo, R. Vlasak, E. Urbach, and D. A. Brian.** 2003. Common RNA replication signals exist among group 2 coronaviruses: evidence for in vivo recombination between animal and human coronavirus molecules. Virology **315:**174–183.
50. **Yee, J. K., T. Friedmann, and J. C. Burns.** 1994. Generation of high-titer pseudotyped retroviral vectors with very broad host range. Methods Cell Biol. **43:**99–112.
51. **Yount, B., K. M. Curtis, E. A. Fritz, L. E. Hensley, P. B. Jahrling, E. Prentice, M. R. Denison, T. W. Geisbert, and R. S. Baric.** 2003. Reverse genetics with a full-length infectious cDNA of severe acute respiratory syndrome coronavirus. Proc. Natl. Acad. Sci. USA **100:**12995–13000.
52. **Yount, B., M. R. Denison, S. R. Weiss, and R. S. Baric.** 2002. Systematic assembly of a full-length infectious cDNA of mouse hepatitis virus strain A59. J. Virol. **76:**11065–11078.
53. **Ziebuhr, J., E. J. Snijder, and A. E. Gorbalenya.** 2000. Virus-encoded proteinases and proteolytic processing in the Nidovirales. J. Gen. Virol. **81:**853–879.
54. **Ziebuhr, J., V. Thiel, and A. E. Gorbalenya.** 2001. The autocatalytic release of a putative RNA virus transcription factor from its polyprotein precursor involves two paralogous papain-like proteases that cleave the same peptide bond. J. Biol. Chem. **276:**33220–33232.